ACS Chemical Neuroscience

Research Article

pubs.acs.org/chemneuro

A Novel Multifunctional Compound Camellikaempferoside B Decreases Aβ Production, Interferes with Aβ Aggregation, and Prohibits Aβ-Mediated Neurotoxicity and Neuroinflammation

Shigao Yang,[†,∥] Wen Liu,[†,§,∥] Shuai Lu,[†,∥] Yong-zhen Tian,[‡] Wei-yun Wang,[*,§] Tie-jun Ling,[*,‡] and Rui-tian Liu[*,†]

[†]National Key Laboratory of Biochemical Engineering, Institute of Process Engineering, Chinese Academy of Sciences, Beijing 100190, China

[‡]State Key Laboratory of Tea Plant Biology and Utilization, Anhui Agricultural University 130 West Changjiang Rd., Hefei 230036, P. R. China

[§]School of Life Science, Anhui Agricultural University, Hefei 230036, China

Supporting Information

ABSTRACT: Accumulating evidence suggested that soluble oligomeric β-amyloid protein (Aβ) exerts diverse roles in neuronal cell death, neuroinflammation, oxidative stress, and the eventual dementia associated with Alzheimer's disease (AD). Developing an agent with multiple properties may be a reasonable strategy for the treatment of AD. In this study, we isolated a novel multifunctional compound named camellikaempferoside B (YCF-2) from Fuzhuan brick tea. YCF-2 consists of kaempferol backbone, *p*-coumaric acid (*p*-CA) group, and a novel structure of rhamnopyranosyl group at the C-4′ position, possessing the properties of both kaempferol and *p*-CA. YCF-2 significantly inhibited Aβ production by decreasing β-secretase activity. Moreover, YCF-2 suppressed Aβ42 fibrillation and facilitated nontoxic oligomer formation by binding to Aβ42 oligomers and by blocking the conformational transition to β-sheet. Furthermore, YCF-2 ameliorated Aβ-induced neuronal cell death, ROS production, inflammatory factor release, and microglia activation by blocking the NF-κB signaling pathway in microglia. These findings indicated that YCF-2 with a novel lead structure has potential applications for drug development for AD treatment.

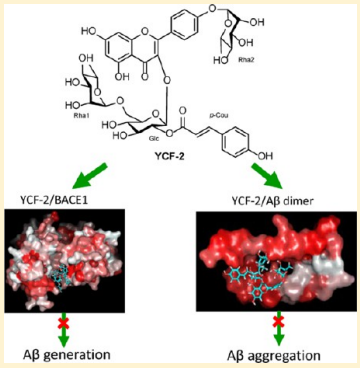

KEYWORDS: *Amyloid-beta, camellikaempferoside B, β-secretase, aggregation, neurotoxicity, microglia*

Alzheimer's disease (AD), the most common form of dementia, is characterized by the accumulation of extracellular plaques of β-amyloid protein (Aβ) and intracellular neurofibrillary tangles of hyperphosphorylated tau protein in the brain.[1] Aβ is derived from the amyloid precursor protein (APP) via successive cleavage by β-secretase (BACE1, beta-site amyloid precursor protein cleavage enzyme) and γ-secretase.[2] Increased Aβ burden leads to the formation of oligomers or fibrils and the deposition of fibrils in the brain parenchyma.[3] Aβ aggregate-mediated cellular processes, including neuronal dysfunction and death,[4,5] neuroinflammation,[6,7] and oxidative stress,[8] have been recognized as early events in the pathogenesis of AD. Increasing experimental evidence indicated that Aβ oligomers are more neurotoxic than fibrils,[4,9,10] whereas fibrils feasibly activate microglia and astrocytes partially through NF-κB signaling. The activated glial cells enhance and amplify neuronal damage induced by Aβ[11,12] and produce proinflammatory cytokines, nitric oxide (NO), and reactive oxygen species (ROS), further promoting neuronal death.[13,14] Therefore, decreasing Aβ production, inhibiting Aβ aggregation and cytotoxicity, and Aβ-mediated inflammation are appealing therapeutics for the treatment of AD.

To inhibit Aβ generation, extensive efforts have been made to target to β- and γ-secretase,[15−18] However, γ-secretase has several other substrates, including Notch 1 and N-cadherin, and therapeutic inhibition of γ-secretase may interfere with physical processes, leading to toxic side effects.[18] BACE1 is a key enzyme for the generation of Aβ and is considered to play a crucial early role in the neurodegenerative and behavioral deficits in AD. Many BACE1 inhibitors were reported to have potential application in AD treatment, with some currently under investigation in clinical trials.[19] To inhibit Aβ aggregation, decrease aggregate formation, and attenuate Aβ cytotoxicity, numerous inhibitors including antibodies, peptides, and synthetic and natural compounds have been tested, but only a few agents are suitable for clinical trials.[18,20] Moreover, many therapeutic efforts have aimed to inhibit Aβ-induced glial inflammation and oxidative stress; some agents show effective therapeutic potential for AD treatment in vitro

Special Issue: Neuroinflammation

Received: March 23, 2016
Accepted: March 25, 2016
Published: March 25, 2016

DOI: 10.1021/acschemneuro.6b00091
ACS Chem. Neurosci. 2016, 7, 505−518

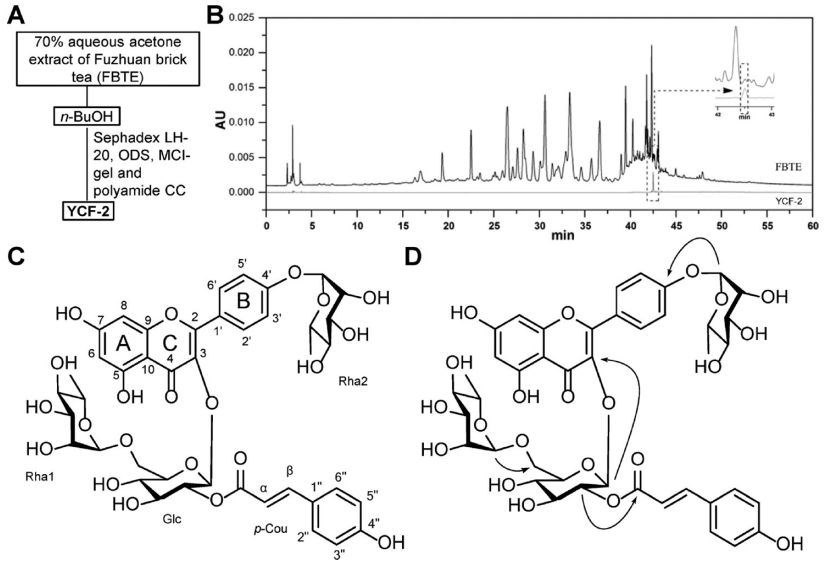

Figure 1. Isolation of YCF-2 from Fuzhuan brick tea. (A) Schematic of the extraction procedure. The *n*-BuOH fraction separated from 70% aqueous acetone extract of Fuzhuan brick tea underwent sequential separation by repeated Sephadex LH-20, ODS, MCI-gel, and polyamide CC to afford YCF-2. (B) HPLC-UV analysis of Fuzhuan brick tea extract (FBTE) and YCF-2. HPLC analyses revealed absorbance at 350 nm. Arrowhead indicates the identified YCF-2. (C) The molecular structure of YCF-2 consists of a kaempferol backbone (A, B, and C rings) with a *p*-coumaroyl (*p*-Cou) linked by a sugar chain. Rha1 and Rha2, rhamnopyranosyl; Glu, glucopyranosyl. (D) Key HMBC correlations of YCF-2 ($^{1}H \rightarrow {}^{13}C$).

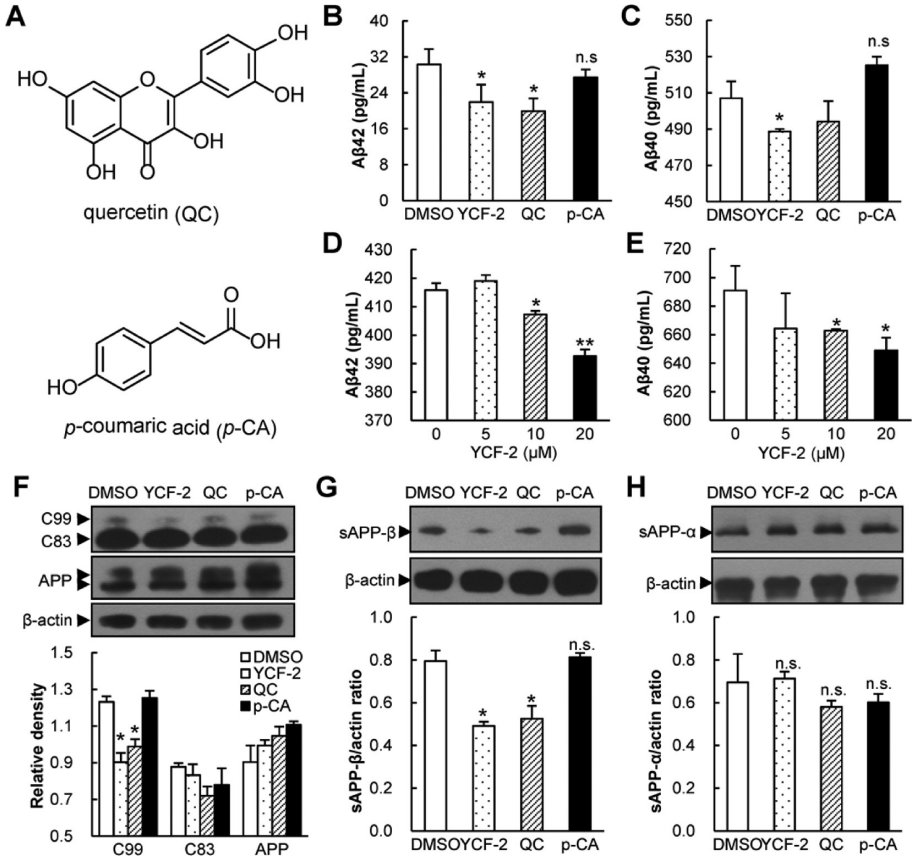

Figure 2. Effect of YCF-2 on APP cleavage and Aβ production in cells. (A) Structure of quercetin (QC) and *p*-coumaric acid (*p*-CA). (B–E) YCF-2 reduced Aβ42 and Aβ40 production. 7PA2 cells were treated with 10 μM YCF-2, QC, and *p*-CA (B, C) or 5, 10, and 20 μM YCF-2 (D, E). The levels of Aβ40 (C, E) and Aβ42 (B, D) in the cell supernatants were analyzed by sandwich ELISA kits. (F–H) YCF-2 decreased the protein levels of C99 (F) and sAPP-β (G), but not APP, C83 (F), and sAPP-α (H). The cell lysates of 7PA2 were further analyzed by Western blot with related antibodies as the primary antibodies and β-actin as a loading control. Bottom, densitometry of the Western blot bands was qualified using ImageJ software and then normalized to β-actin (compared with cell controls; *, $p < 0.05$; **, $p < 0.01$; n.s., not significant).

DOI: 10.1021/acschemneuro.6b00091
ACS Chem. Neurosci. 2016, 7, 505–518

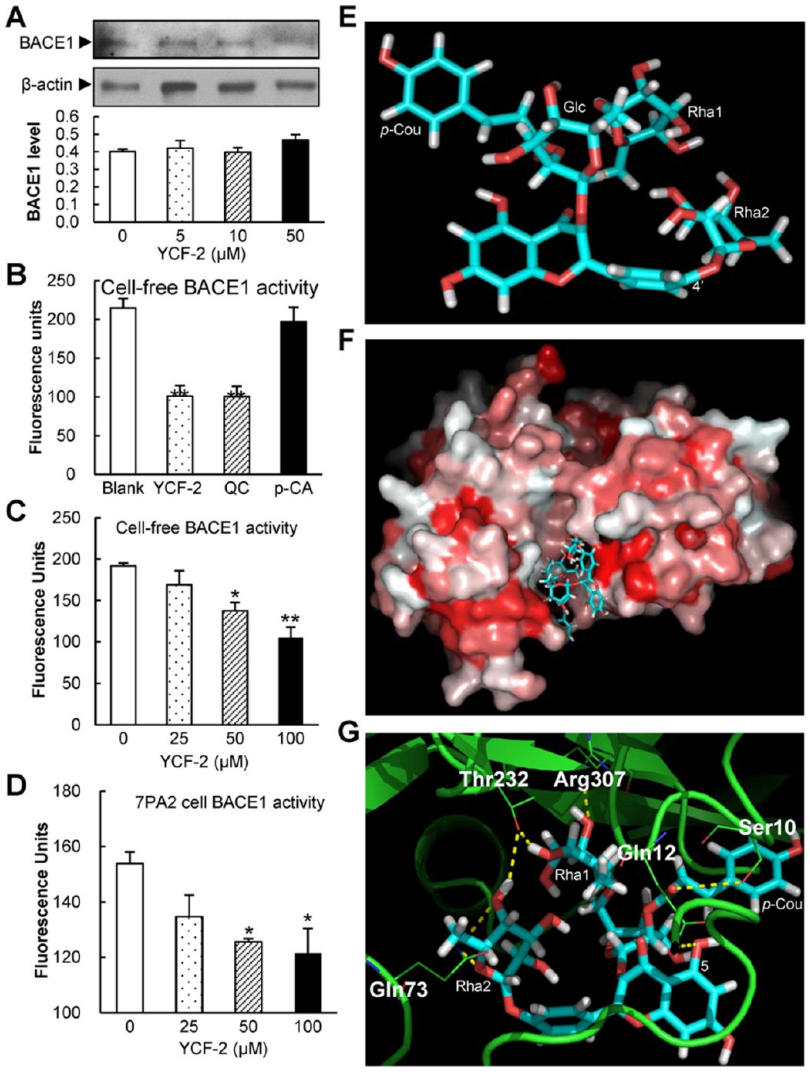

Figure 3. YCF-2 may inhibit BACE1 activity by binding to its active sites. (A) YCF-2 had no effect on the protein expression of BACE1. 7PA2 cells were treated with different concentrations of YCF-2, and the BACE1 protein levels in 7PA2 lysates were detected by Western blot with β-actin as a loading control. Bottom, densitometry of the bands was normalized to β-actin and represented the relative protein levels. (B and C) YCF-2 inhibited BACE1 activity in a cell-free system. YCF-2, QC, and *p*-CA (100 μM) (B) or different concentrations of YCF-2 (C) were preincubated with 0.5 μg of BACE1 in a reaction buffer for 20 min. The substrate was added and incubated for 1 h. Fluorescence was measured at excitation and emission wavelengths of 350 and 500 nm, respectively. Relative fluorescence units are shown on the *y*-axis. Each experiment was performed in triplicate. (D) YCF-2 inhibited BACE1 activity in 7PA2 cells. 7PA2 cells were treated with different concentrations of YCF-2 for 24 h, and the cell lysates were collected for the detection of BACE1 activity. The fluorescence was measured as described in (C) (compared with cell controls; *, $p < 0.05$; **, $p < 0.01$). (E) Stick model of YCF-2 deduced from molecular dynamics. (F) The complex structure of BACE1 and YCF-2 molecules obtained from molecular dynamics simulation. (G) Interactions between the YCF-2 and the active sites of BACE1.

and in vivo.[21,22] Given that AD is a complex, multifactorial neurodegenerative disease, the currently available one-target strategies may be insufficient to impede the pathological processes of AD. Therefore, the screening of multifunctional agents that can hit multiple targets simultaneously is attracting much effort.[16,23]

Some multifunctional agents, including organic compounds,[24,25] peptides,[26,27] and antibodies,[28,29] were reported to prevent Aβ production and aggregation, reduce Aβ-mediated cytotoxicity, and decrease the inflammatory response. Several natural compounds extracted from herbs or functional foods, such as tea, have received particular attention because of their safety and therapeutic potential in vitro and in vivo. EGCG,[30,31] resveratrol,[28,32,33] and curcumin[34] were reported to bind to monomeric Aβ or toxic aggregates, leading to conformational changes in the β-sheet-rich assemblies and to form less toxic amyloid species. Moreover, flavonoids, especially quercetin (QC), exhibited neuroprotective properties in AD via multiple mechanisms, including antiamyloid aggregation,[35] anti-BACE1 activity,[36] and antioxidative effect[37] and AMPK activation.[38] In the present paper, we report the multiple effects of camellikaempferoside B (also named YCF-2), a novel natural compound, containing kaempferol backbone and *p*-coumaric acid (*p*-CA) and rhamnopyranosyl groups, isolated from Fuzhuan brick tea (FBT), on Aβ production and aggregation, as well as Aβ-mediated cytotoxicity and neuroinflammation.

RESULTS AND DISCUSSION

Isolation and Characterization of YCF-2. The 70% aqueous acetone extract of FBT was separated successively by petroleum ether, $CHCl_3$, and *n*-BuOH. The *n*-BuOH fraction

DOI: 10.1021/acschemneuro.6b00091
ACS Chem. Neurosci. 2016, 7, 505−518

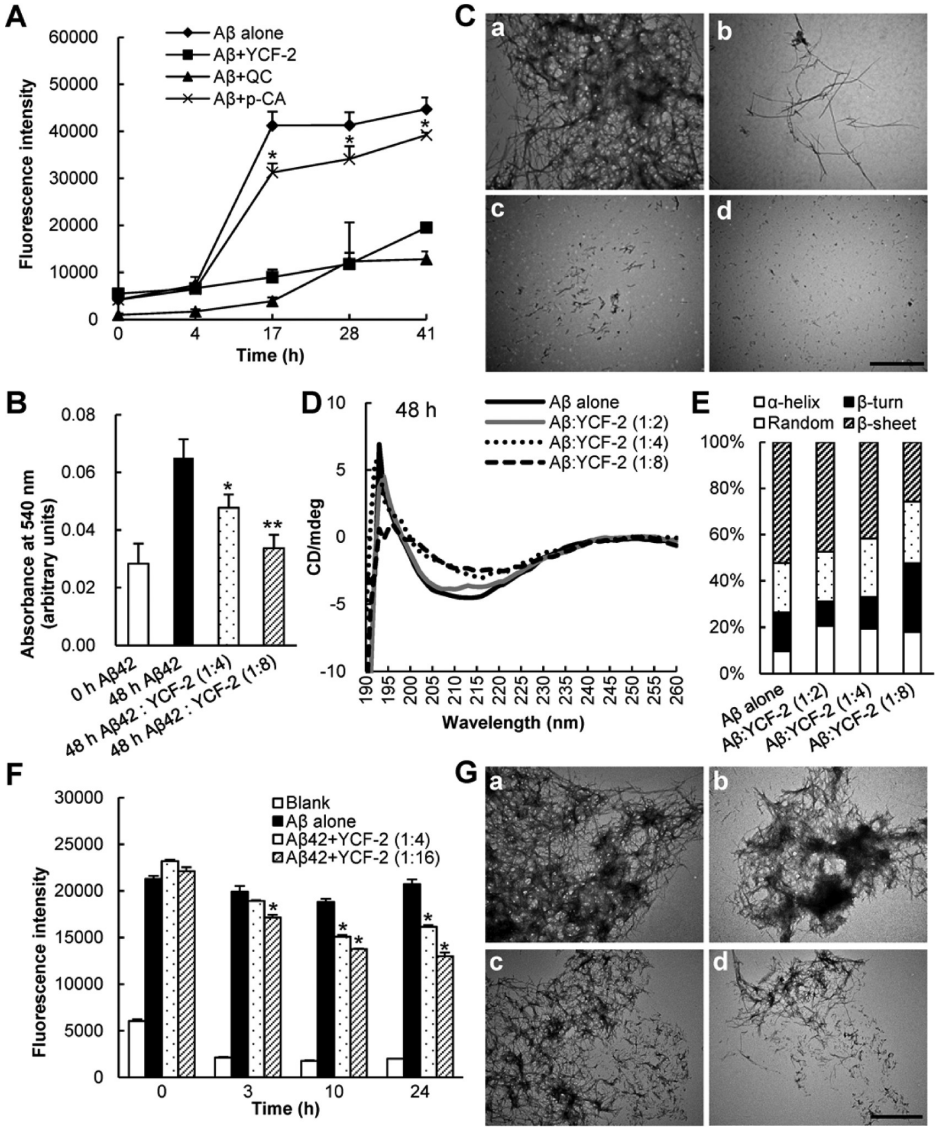

Figure 4. Effect of YCF-2 on Aβ42 fibrillation. (A) YCF-2 inhibited Aβ42 fibril formation. Aβ42 (20 μM) fibril formation was monitored by ThT fluorescence in the absence and presence of YCF-2, QC, or *p*-CA at a ratio of 1:4. Fluorescence intensity was measured at excitation and emission wavelengths of 450 and 482 nm, respectively. (B) Inhibitory effect of YCF-2 on of Aβ42 fibrillation detected by Congo red (CR). CR absorbance was measured in the absence or presence of 20 μM Aβ42 at 540 nm (Aβ42:YCF-2 at the ratio of 1:0, 1:4 and 1:8). CR (20 μM) was immediately added to the samples before reading the absorbance (compared with 48 h incubated Aβ42 alone; *, $p < 0.05$, **, $p < 0.01$). (C) Morphologies of 20 μM Aβ42 samples incubated alone (a) or with 80 (b), 160 (c), and 320 μM (d) YCF-2 were examined using a Hitachi H7650 TEM at 80 kV. The scale bar is 1 μm. (D and E) YCF-2 blocked β-sheet formation during Aβ42 aggregation. The CD spectra of Aβ42 incubated with or without different concentrations of YCF-2 (40, 80, and 160 μM) were recorded at 48 h in the spectral range of 190−260 nm. The data were the mean of two independent experiments. Percentages of different secondary structures were analyzed by the Protein Secondary Structure Estimation Program (E). (F) YCF-2 promoted the disaggregation of preformed Aβ42 fibrils. Preformed Aβ42 fibrils (20 μM) were monitored by ThT fluorescence in the absence and presence of YCF-2 at a ratio of 1:4 or 1:16 at different time points with excitation and emission wavelengths of 450 and 482 nm, respectively (compared with Aβ42 alone; *, $p < 0.05$). (G) Morphologies of 20 μM Aβ42 fibril samples incubated alone (a) or with 80 (b), 160 (c), and 320 μM (d) YCF-2 for 24 h were examined using a Hitachi H7650 TEM at 80 kV. The scale bar is 1 μm.

was separated by repeated Sephadex LH-20, ODS, MCI-gel, and polyamide CC to afford YCF-2 (Figure 1A). The occurrence of YCF-2 in the Fuzhuan brick tea extract (FBTE) was confirmed by HPLC-UV analysis (Figure 1B).

YCF-2 was isolated as a yellow amorphous powder. Its UV spectrum exhibited two characteristic flavonol absorption bands at 314 and 268 nm (Figure S1). The characteristic absorption bands of the IR spectrum were 3380, 2918, 2850, 1697, 1649, 1604, 1506, 1358, 1246, 1174, 1133, 1062, 981, 834, 670, 599, 577, 482, and 439 nm (Figure S2). The HRESI-MS spectrum showed the $[M - H]^-$ signal at m/z 885.2424 (Figure S3), corresponding to the molecular formula of $C_{42}H_{46}O_{21}$. The NMR data of YCF-2 were very similar to those of kaempferol-3-*O*-β-D-(*p*-coumaroyl)-rutinoside, except for the additional data on a rhamnopyranosyl [δ_H 5.540 (1H, br s) and 1.135 (3H, d, J = 6.2 Hz), δ_C 98.12 (C-Rha2-1), 70.19 (C-Rha2-2), 70.31 (C-Rha2-3), 71.75 (C-Rha2-4), 73.91 (C-Rha2-), and 17.71 (C-Rha2-6)][18] (Table S1, Figures S4−S7). This rhamnopyranosyl group was indicated to be at the C-4′ position by a long-range correlation between 5.540 (1H, br s, H-Rha2-1) and 157.91 (C-4′) (Table S1, Figure 1C). The connections between coumaroyl and the remaining glycosyls

DOI: 10.1021/acschemneuro.6b00091
ACS Chem. Neurosci. 2016, 7, 505−518

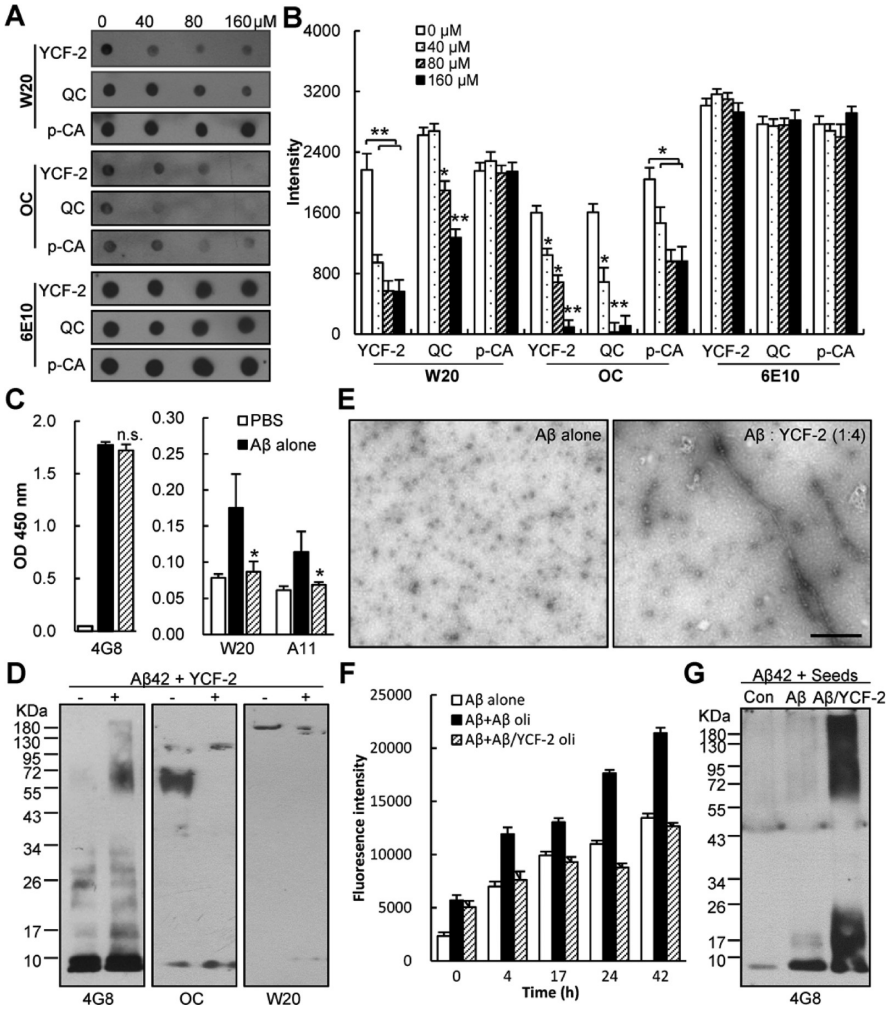

Figure 5. Effect of YCF-2 on Aβ42 oligomerization. (A–C) YCF-2 suppressed W20-, OC-, and A11-positive oligomer formation. Aβ42 incubated with or without YCF-2, QC, and *p*-CA was spotted on a nitrocellulose membrane. Aβ42 oligomers were detected by dot blot assay using oligomer-specific antibodies W20, OC, and A11 or anti-Aβ1-16 antibody 6E10 as the primary antibodies (A). Densitometry of the dots was qualified using IpWin5 (B). (C) Measurement of Aβ42 oligomer levels by ELISA. The microtiter plate was coated with Aβ42 samples preincubated with or without YCF-2. After blocking, bound Aβ42 oligomers were detected by W20, A11, and 4G8. (D and E) YCF-2 promoted oligomer formation. Aβ42 incubated with or without YCF-2 for 4 h was examined by Western blot with indicated antibodies (D) and TEM (E). The scale bar is 500 nm. (F and G) YCF-2-induced Aβ42 oligomers failed to accelerate Aβ42 fibrillation but promoted oligomer formation. Aβ42 incubated with or without YCF-2 for 4 h as a "seed" was added to Aβ42 monomers at the ratio of 1:10. ThT dye (F) and Western blot (G) were applied to detect the fibrils and oligomers (compared with Aβ42 alone; *, $p < 0.05$; **, $p < 0.01$; n.s., not significant).

were confirmed by the HMBC cross peaks between the signals of δ_H 5.530 (1H, d, J = 8.0 Hz, H-Glc-1) and δ_C 133.19 (C-3), δ_H 4.830 (1H, dd, J = 8.2, 9.4 Hz, H-Glc-2) and δ_C 165.81 (C-Cou-CO), as well as δ_H 4.35 (1H, br s, H-Rha1-1) and δ_C 66.99 (C-Glc-6), respectively (Table S1, Figure 1D, Figure S8). Chemical derivatization were determined by acid hydrolysis, trimethylsilylimidazole derivation and GC-MS analysis. The results indicated that the configurations of glucosyl and rhamnosyl were D and L, respectively, (Figures 1D and S9). Collectively, YCF-2 was identified as kaempferol-3-*O*-[*E*-*p*-coumaroyl-(1 → 2)][α-L-rhamnopyranosyl-(1 → 6)]-β-D-glucopyranoside-4′-*O*-α-L-rhamnopyranoside. This novel compound was trivially named Camellikaempferoside B. To compare the activities of YCF-2 with its components, QC (Figure 2A), which contains very similar structure to kaempferol and has been extensively studied, and *p*-CA were used in the following experiment.

YCF-2 Reduces Aβ Production via Inhibiting β-Secretase Activity. To determine the effect of YCF-2 on APP metabolism and Aβ production, 7PA2 cells were treated with YCF-2, QC, and *p*-CA. Sandwich ELISA results showed that YCF-2 and QC, but not *p*-CA, decreased the levels of Aβ42 and Aβ40 (Figure 2B and C), and YCF-2 inhibited the formation of Aβ42 and Aβ40 in a dose-dependent manner (Figure 2D and E). We next explored the mechanism by which YCF-2 decreased Aβ generation. Our results showed that YCF-2 and QC, rather than *p*-CA, reduced the protein levels of amyloidogenic C99, but not those of nonamyloidogenic C83 and APP (Figure 2F). Consistently, YCF-2 and QC significantly decreased the protein level of sAPP-β, but not that of sAPP-α (Figure 2H). These results indicated that YCF-2 reduced APP hydrolysis by inhibiting β-cleavage on APP.

To determine whether YCF-2 inhibited β-cleavage on APP through directly targeting BACE1, we first detected the BACE1 protein levels in 7PA2 cells after YCF-2 treatment. The results showed that YCF-2 did not interfere with the expression of BACE1 (Figure 3A). QC[36] and *p*-CA[39] were previously reported to suppress BACE1 activity in vitro. We then

DOI: 10.1021/acschemneuro.6b00091
ACS Chem. Neurosci. 2016, 7, 505–518

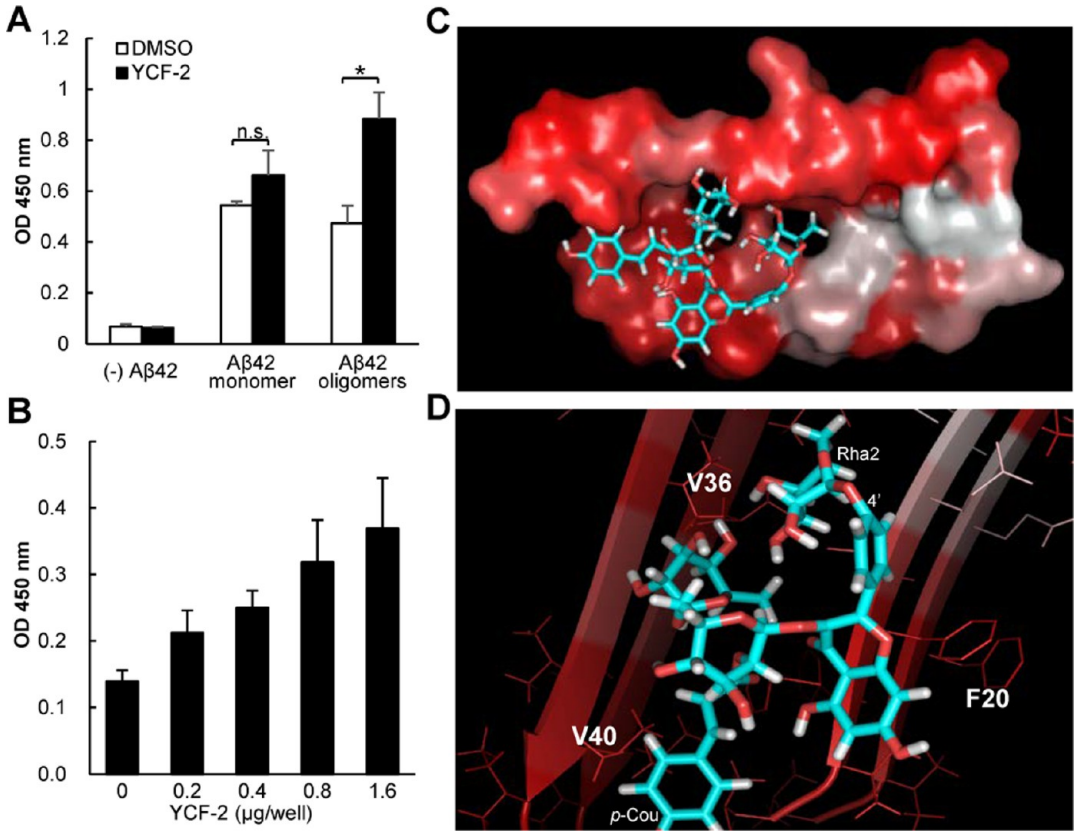

Figure 6. YCF-2 directly interacts with Aβ42. (A, B) ELISA detected the interaction of YCF-2 and Aβ42. Microtiter plates were coated with YCF-2. After blocking, 500 ng of Aβ42 monomers (A) or Aβ42 oligomers (A, B) were added to each well. The bound Aβ was detected by 4G8 antibody followed by a secondary antibody conjugated with horseradish peroxidase (compared with DMSO control; *, $p < 0.05$; n.s., not significant). (C) Frontal views of the complex structure of Aβ17−42 dimer and YCF-2 molecule obtained from molecular dynamics simulation. (D) Interactions between the flavanone ring in YCF-2 and the phenyl ring of Phe20 of the Aβ17−42 dimer.

determined whether YCF-2 affected BACE1 activity in a cell-free system. Our results showed that YCF-2 and QC, but not *p*-CA, reduced BACE1 activity, and YCF-2 decreased BACE1 activity in a dose-dependent manner (Figure 3B and C). Consistently, BACE1 activity in 7PA2 cells treated with YCF-2 was significantly reduced (Figure 3D), suggesting that YCF-2 might reduce Aβ production by inhibiting BACE1 activity. Previous studies showed that flavonoids directly interact with the BACE1 catalytic center and reduce APP amyloidogenic hydrolysis.[36] To further elucidate the mechanism by which YCF-2 inhibited BACE1 activity, we employed molecular docking simulation. The results showed the molecular structure of YCF-2 (Figure 3E) and a complete view of the docking pose of YCF-2 toward BACE1 (Figure 3F). YCF-2 formed five hydrogen bonds to Gln73, Thr232, and Arg307 by its Rha1 and Rha2, and also formed one hydrogen bond between C5-OH of the A ring and Gln12. In addition, YCF-2 formed a hydrogen bond between Ser10 and *p*-Cou (Figure 3G). Collectively, these results suggested that the interaction between YCF-2 and several active sites of BACE1 via hydrogen bonds may lead to the decrease in BACE1 activity and Aβ production.

YCF-2 Inhibits Aβ Fibrillation and Promotes Preformed Fibril Disaggregation. Previous studies revealed that Aβ oligomers are more toxic to neurons than fibrils,[4,9,10] but Aβ fibrils may provide a catalytic surface for the continuous generation of toxic oligomers.[40,41] Our ThT fluorescence assay showed that YCF-2 and QC, but not *p*-CA, exerted obvious inhibitory effects on Aβ42 aggregation (Figure 4A). Consistent with the ThT fluorescence results, CR absorbance at 540 nm in Aβ alone sample was obviously increased after incubation, whereas the addition of YCF-2 significantly decreased the CR absorbance in a concentration-dependent manner (Figure 4B). TEM results showed that 20 μM Aβ42 aggregated to numerous fibrils after 24 h of incubation, whereas Aβ42 coincubated with 80 μM YCF-2 formed a few fibrils. Several short fibrils were observed in Aβ42 samples with 160 μM YCF-2, whereas only oligomers were detected when Aβ42 was incubated with 320 μM YCF-2 (Figure 4C), suggesting that YCF-2 inhibits Aβ fibrillation.

The formation of β-sheet was shown to be a crucial step in Aβ fibrillation. To investigate the effect of YCF-2 on the conformational conversion of Aβ42, representative CD spectra of Aβ42 coincubated with or without YCF-2 for 48 h were analyzed. The CD spectra of Aβ42 after incubation displayed a strong positive peak and a negative peak at around 195 and 215 nm, respectively (Figure 4D). However, the typical CD spectra of Aβ42 were impaired by YCF-2 treatment (Figure 4D), and the percentage of β-sheet in Aβ showed obvious changes with the addition of YCF-2 (Figure 4E). These results indicated that YCF-2 inhibits Aβ fibrillation by reducing β-sheet structure formation.

Removing or disaggregating preformed Aβ fibrils is another therapeutic strategy in AD. To investigate the effect of YCF-2 on mature Aβ42 fibrils, ThT fluorescence assay and TEM were applied to monitor Aβ42 fibrils incubated with or without YCF-

DOI: 10.1021/acschemneuro.6b00091
ACS Chem. Neurosci. 2016, 7, 505−518

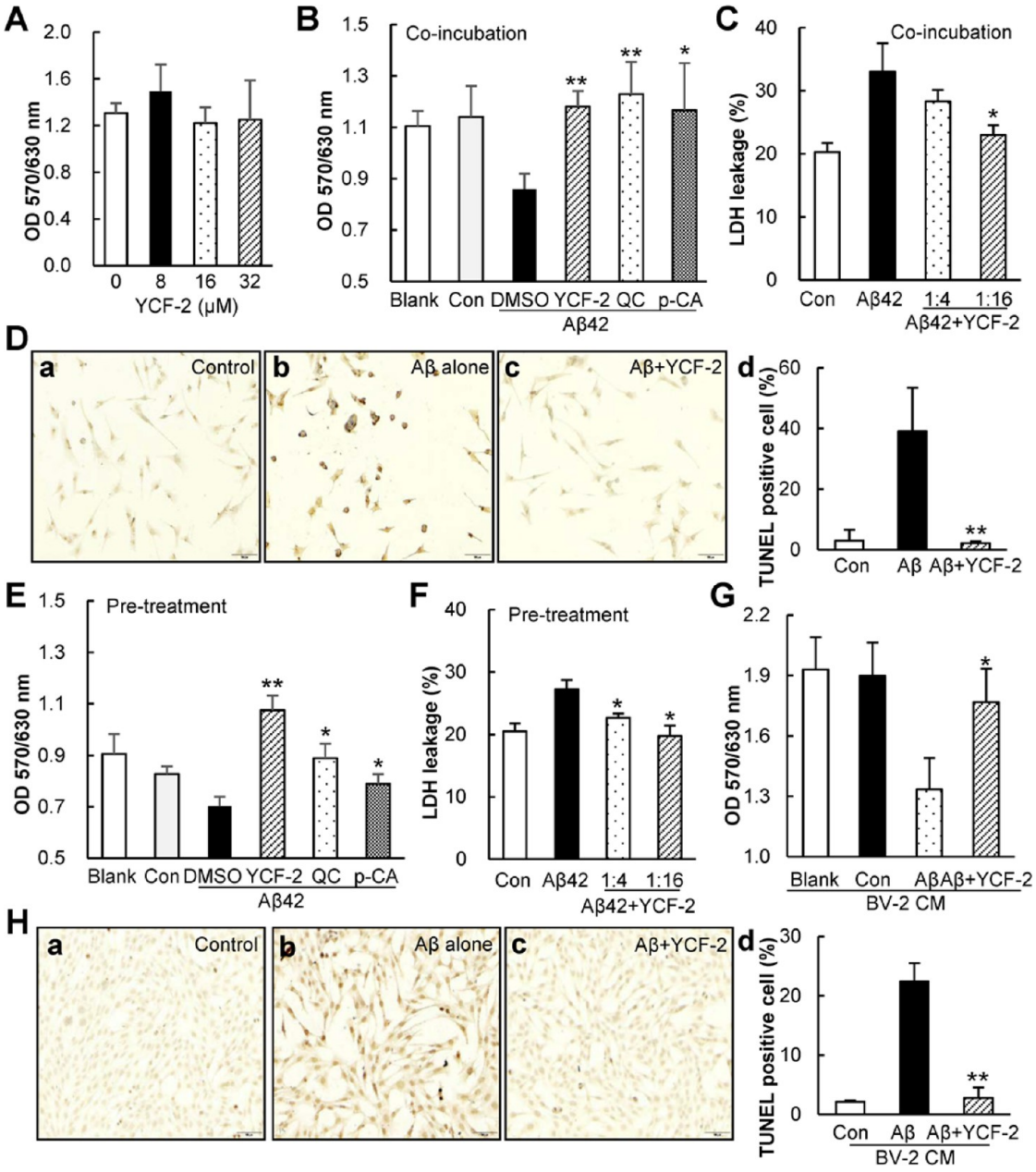

Figure 7. Effect of YCF-2 on Aβ42-induced HT22 neuronal cell death. (A–F) YCF-2 inhibited Aβ42-induced HT22 cell death. HT22 cells were incubated with YCF-2 alone (A) or Aβ42 coincubated with or without YCF-2, QC, and *p*-CA (B–D), or were pretreated with or without YCF-2, QC, and *p*-CA, and then stimulated with Aβ42 oligomers (E, F). Cell viability was detected with MTT (A, B, E) and LDH (C, F) assays. Apoptotic cell death was assessed with TUNEL assay (D, H). Data are presented as the mean ± SD of three independent experiments (compared with Aβ alone; *, $p < 0.05$; **, $p < 0.01$). (G, H) YCF-2 suppressed microglia-mediated neuronal cell death. BV-2 cells were treated with Aβ42 in the absence or presence of YCF-2 for 24 h, and the cell-free supernatant was added to HT22 cells. After 24 h of incubation, the viability and apoptotic cell death of HT22 cells were detected by MTT assay (G) and TUNEL assay (H), respectively (compared with Aβ alone; *, $p < 0.05$; **, $p < 0.01$).

2. A remarkable reduction in ThT fluorescence and less fibrils were observed with the addition of YCF-2 (Figure 4F and G).

YCF-2 Facilitates the Formation of Abnormal Aβ Oligomers. Aβ oligomers are more toxic to neurons than Aβ fibrils and play a more important role in the pathological processes of AD. To determine the effect of YCF-2 on Aβ oligomerization, dot blot assay was performed to detect oligomer levels in Aβ42 coincubated with or without YCF-2, QC, and *p*-CA using oligomer-specific antibodies W20,[28] OC,[42] and A11.[43] The results showed that YCF-2 and QC, rather than *p*-CA, significantly decreased the levels of W20- and OC-positive oligomers, whereas *p*-CA reduced the levels of OC-positive but not W20-positive oligomers (Figure 5A and B). Consistently, our ELISA results showed that YCF-2 also significantly decreased the levels of W20- and A11-positive oligomers (Figure 5C). Furthermore, our Western blot and TEM results showed that Aβ42 alone aggregated to a few oligomers after 4 h incubation, whereas Aβ42 incubated with YCF-2 formed bigger oligomers (Figure 5D and E). However, these oligomers induced by YCF-2 failed to be recognized by OC and W20 (Figure 5D). These results suggested that YCF-2 promoted Aβ oligomerization, but the formed oligomers were structurally distinct from that formed by Aβ42 alone.

DOI: 10.1021/acschemneuro.6b00091
ACS Chem. Neurosci. 2016, 7, 505–518

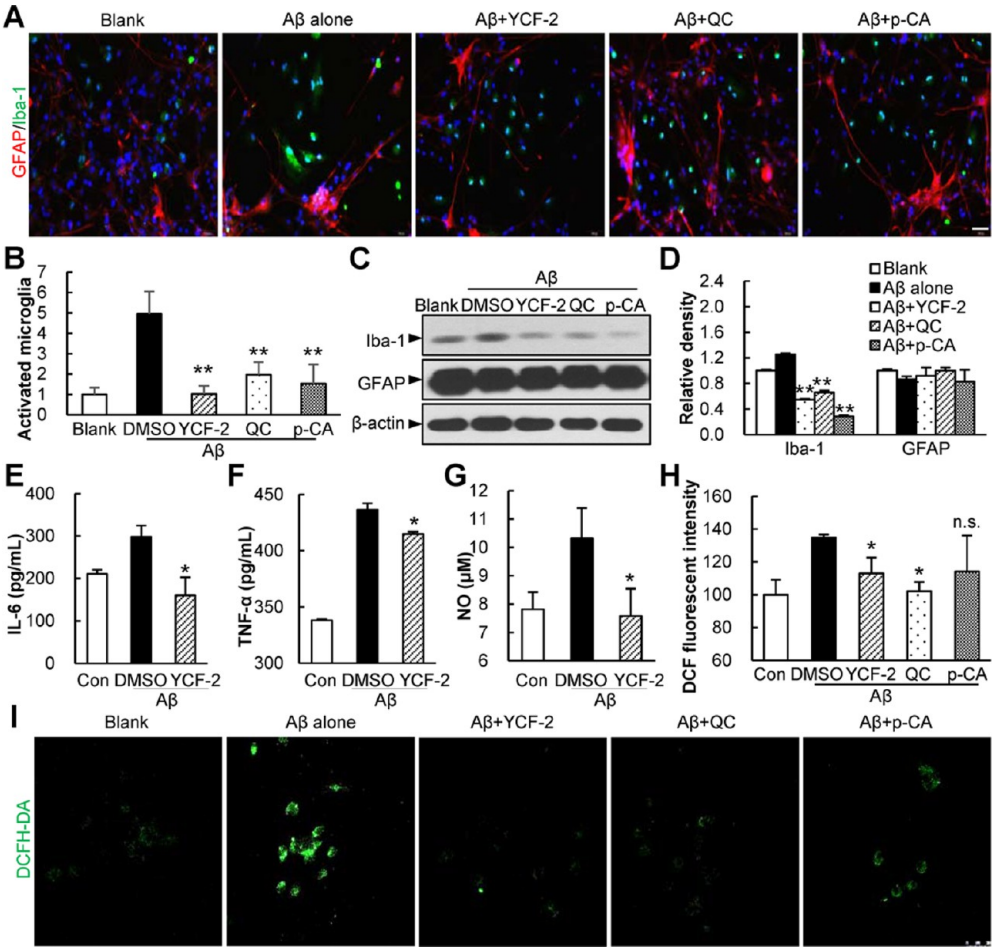

Figure 8. YCF-2 inhibits Aβ42-induced microglial activation, inflammatory molecule release, and ROS production. (A–D) YCF-2 suppressed Aβ42-induced primary microglial activation and decreased the protein level of Iba-1. Glial cells were treated with vehicle (blank) or 5 μM Aβ42 mixed with or without YCF-2, QC, and *p*-CA for 24 h. Cells were fixed and analyzed by double immunostaining with anti-Iba-1 (green) and anti-GFAP (red) antibodies. The nuclei were stained by DAPI (blue) (bars represent 50 μm) (A). Activated microglial cells with large cell bodies were qualified using IpWin5 and then normalized to blank (B). Microglial lysates were examined by Western blot using Iba-1 and GFAP antibodies (C). The relative density of Iba-1 from three independent experiments was quantified, normalized to β-actin, and presented as the mean ± SD (D) (compared with Aβ alone; **, $p < 0.01$). (E–G) YCF-2 inhibited the production of neuroinflammatory molecules in Aβ42-stimulated BV-2 cells. BV-2 cells were treated with 5 μM Aβ42 mixed with or without YCF-2 for 24 h. The concentrations of IL-6 (E), TNF-α (F), and NO (G) in the media were measured using ELISA kits (compared with Aβ alone; *, $p < 0.05$). (H, I) YCF-2 inhibits Aβ42-induced ROS production in BV-2 cells. Cells were treated with 5 μM Aβ42 without or with YCF-2, QC, and *p*-CA for 24 h, and then incubated with DCFH-DA for 30 min. The intracellular levels of ROS were then determined using a fluorometer (H) and confocal microscopy (I). The values represent the relative fluorescence intensity from three independent experiments (compared with Aβ alone; *, $p < 0.05$) (H).

Previous reports indicated that the preformed Aβ oligomers act as "seeds" to accelerate Aβ aggregation. We then determined the effect of the preformed YCF-2-mediated Aβ oligomers on Aβ aggregation. Our ThT dyeing results showed that the addition of normal Aβ oligomers obviously enhanced the fluorescence intensity of Aβ42, whereas YCF-2-mediated Aβ oligomers failed to promote ThT fluorescence of Aβ (Figure 5F), but induced more oligomer formation (Figure 5G). These results suggested that the structures of Aβ42 oligomers induced by YCF-2 might be different from that of normal Aβ42 oligomers. Many compounds have been reported to prevent the formation of toxic Aβ oligomers by inhibiting oligomerization, stabilizing small nontoxic oligomers,[44] promoting the formation of nontoxic β-sheet-rich amyloid fibrils,[45] or remodeling mature fibrils into unstructured aggregates.[46] Our present results demonstrated that YCF-2 mediated Aβ42 monomers into abnormal Aβ oligomers with few β-sheet structures, and inhibited Aβ42 fibrillation by stabilizing these preformed Aβ oligomers.

YCF-2 Directly Binds to Aβ42. To detect the interaction of YCF-2 with Aβ42, ELISA assay was carried out with YCF-2 coated to ELISA plates. The plates were incubated with Aβ42 monomer or oligomers, and bound Aβ42 was detected with 4G8. The results showed that YCF-2 preferred to bind to Aβ42 oligomers rather than Aβ42 monomer (Figure 6A). The amount of bound Aβ42 oligomers was positively correlated with coated YCF-2 in a dose-dependent manner (Figure 6B). To further investigate the molecular details of the interactions between YCF-2 and Aβ42, molecular dynamics simulations were performed. The atomic contacts between YCF-2 and oligomeric Aβ17–42 dimer were calculated to simulate the interactions between YCF-2 and Aβ42 oligomers. The snapshots of simulated results showed that YCF-2 was integrated into oligomeric Aβ17–42 dimers, and partial groups of YCF-2 were almost embedded into the hydrophobic holes of

DOI: 10.1021/acschemneuro.6b00091
ACS Chem. Neurosci. 2016, 7, 505–518

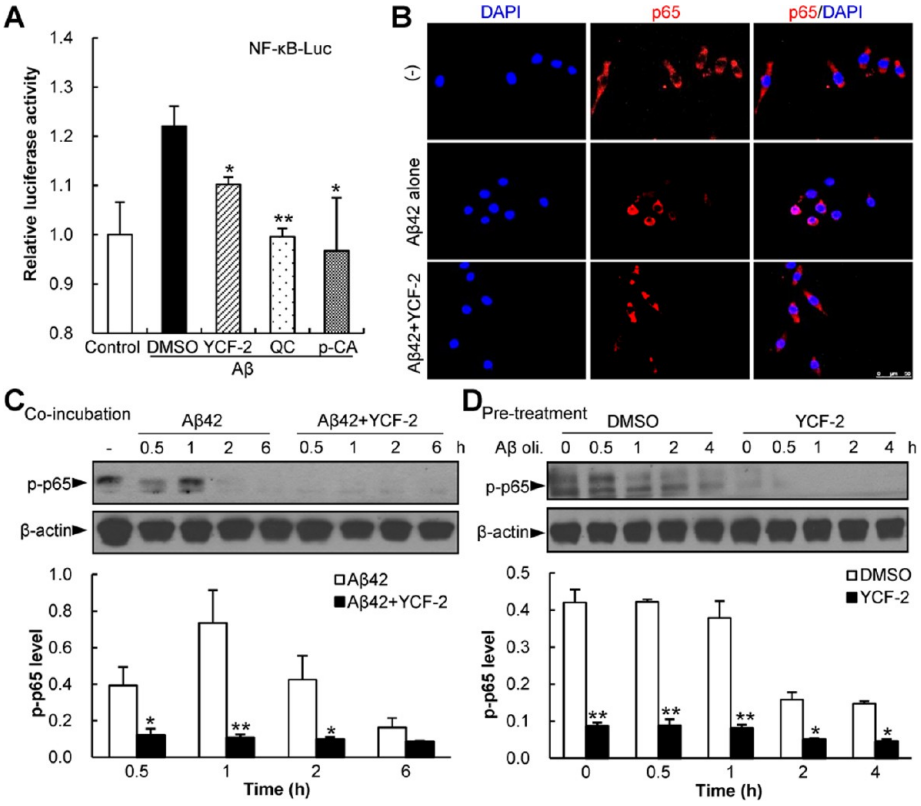

Figure 9. YCF-2 inhibits Aβ42-induced NF-κB activation in BV-2 microglial cells. (A) YCF-2 reduced NF-κB transcriptional activity induced by Aβ42 oligomers. BV-2 cells were transfected with NF-κB luciferase reporter and pRL-TK, and then stimulated with Aβ42 in the absence or presence of YCF-2, QC, and *p*-CA. Luciferase activity was measured using a dual-luciferase reporter assay system. (B) YCF-2 inhibited the Aβ42-induced p65 nuclear translocalization. BV-2 cells were treated with Aβ42 mixed with or without YCF-2 for 15 min (bars represent 50 μm). (C, D) YCF-2 suppressed the levels of phosphorylated p65 in BV-2 cells stimulated with Aβ42. BV-2 cells were treated with Aβ42 coincubated with or without YCF-2 (C), or pretreated with or without YCF-2 (D), and then stimulated with Aβ42 oligomers at the indicated time points. The endogenous phosphorylated status of p65 was examined by Western blot. Bottom, densitometry of the bands was qualified using ImageJ software and then normalized to β-actin (compared with Aβ alone; *, $p < 0.05$; **, $p < 0.01$).

Aβ-Aβ (Figure 6C). The simulation results showed that YCF-2 preferentially interacted with Phe20, Val36, and Val40 over others in Aβ17−42 (Figure 6D). Detailed analysis revealed that the flavanone ring of YCF-2 bound directly with the phenyl rings of Phe20 through $\pi-\pi$ stacking. In addition, strong hydrophobic interactions were found between the *p*-coumaroyl group (*p*-Cou) of YCF-2 and Val40 of Aβ42. The hydroxyl groups within the rhamnopyranosyl group (Rha2) at the C-4′ position of YCF-2 were bound to Val36 of Aβ42 through hydrogen bonding (Figure 6D). Collectively, these results suggested that the interaction between YCF-2 and Aβ42 via hydrophobic associations, $\pi-\pi$ stacking, and hydrogen bonding might be responsible for the inhibition of Aβ42 fibrillation and the formation of abnormal Aβ aggregates.

YCF-2 Decreases Aβ-Induced Neuronal Cell Death. QC and p-CA were shown to inhibit Aβ cytotoxicity.[35,47] To determine the cytotoxicity of Aβ oligomers modulated by YCF-2 to HT22 hippocampal cells, we conducted MTT, LDH and TUNEL assays to measure cell viability and apoptosis. When HT22 hippocampal cells were treated with different concentrations of YCF-2, they showed no obvious changes in cell viability, suggesting that YCF-2 was not toxic to HT22 cells (Figure 7A). Aβ42 obviously decreased crystal production and increased LDH release, whereas YCF-2, QC, or *p*-CA significantly attenuated Aβ42-induced neurotoxicity (Figure 7B and C). Consistently, when Aβ42 mixed with YCF-2 was added to the cell culture, YCF-2 markedly inhibited Aβ42-induced apoptotic cell death (Figure 7D), indicating that Aβ42 oligomers mediated by YCF-2 demonstrated low cytotoxicity. Moreover, pretreatment of HT22 cells with YCF-2, QC, or *p*-CA also protected cells from the toxicity induced by Aβ42 oligomers by increasing crystal generation (Figure 7E) and decreasing LDH release (Figure 7F). These results suggested that the flavanone ring and p-coumaroyl group played a vital role in the inhibition of Aβ cytotoxicity. Previous studies demonstrated that activated microglia exert indirect toxicity to neuronal cells.[11,12] In the present study, we treated BV-2 microglial cells with Aβ oligomers for 24 h and then removed the supernatant of the culture media to HT22 cells. The MTT and TUNEL results showed that HT22 cells displayed lower viability and more cell death than the controls, whereas the cultured BV-2 media treated with Aβ42 in the presence of YCF-2 showed lower neurotoxicity (Figures 7G and 7H). Thus, YCF-2 may prevent microglia-mediated neuronal cell death.

YCF-2 Suppresses Aβ-Induced Neuroinflammation and Oxidative Stress. Activated microglia-mediated neurotoxicity and inflammation contribute to AD pathogenesis.[11−14] To investigate the effect of YCF-2 on Aβ-induced neuroinflammation and oxidative stress, the mixed primary glial cells were stimulated with Aβ in the absence or presence of YCF-2, QC, *p*-CA, and the glial morphologies and Iba-1 protein levels were detected. Aβ stimulation enlarged the cell bodies of

DOI: 10.1021/acschemneuro.6b00091
ACS Chem. Neurosci. 2016, 7, 505−518

microglia and astrocytes, indicating that Aβ simultaneously activated microglia and astrocytes, whereas YCF-2, QC, and *p*-CA significantly suppressed Aβ-induced morphological changes in microglia but not astrocytes (Figure 8A and B). Consistently, Aβ42 enhanced the protein levels of Iba-1 in the mixed primary glia cells, whereas YCF-2, QC, and *p*-CA attenuated the Aβ-induced effect. However, Aβ42, YCF-2, QC, and *p*-CA did not affect GFAP protein levels (Figure 8C and D). These results suggested that YCF-2 inhibited Aβ-induced microglial activation.

Overactivation of microglia may result in the production of proinflammatory mediators and oxidative damage, which can contribute to the pathological processes of AD. To further determine the effect of YCF-2 on Aβ-induced neuroinflammation, we measured the levels of proinflammatory factors in BV-2 cells activated by Aβ42 in the absence or presence of YCF-2. Aβ42 alone markedly increased the levels of IL-6, TNF-α, and NO in BV-2 cells, whereas YCF-2 significantly attenuated the Aβ42-induced increase in proinflammatory factors (Figure 8E−G). To study the effect of YCF-2 on Aβ-induced ROS production in microglia, we detected intracellular ROS using the fluorescence reagent CM-H_2DCFDA for fluorometry and confocal microscopy. Consistent with previous studies, Aβ increased ROS levels in BV-2 cells (Figure 8H and I). However, the addition of YCF-2 or QC significantly suppressed Aβ-induced ROS generation. *p*-CA also decreased the ROS levels, but no statistical difference was found. In conjunction with previous reports and our results that QC and *p*-CA inhibited Aβ-induced microglial activity, suppressed ROS production, and inhibited NF-κB activity in BV-2 microglial cells,[48−50] we may conclude that the structures of kaempferol and *p*-CA played a vital role in inhibiting neuroinflammation. Collectively, these results demonstrated that YCF-2 inhibited microglial activation and suppressed the production of proinflammatory mediators and oxidative stress, which may decrease Aβ-stimulated neuronal cell death.

YCF-2 Inhibits Aβ-Induced NF-κB Activation. NF-κB activation plays a critical role in microglial activation and the expression of proinflammatory mediators. To explore the effect of YCF-2 on the NF-kB signaling pathway in Aβ-stimulated microglia, we detected luciferase activity and p65 levels in Aβ-stimulated microglial cells in the absence and presence of YCF-2, QC, and *p*-CA. Aβ obviously enhanced luciferase activity, whereas YCF-2, QC, and *p*-CA suppressed Aβ-induced NF-κB transcriptional activity (Figure 9A). Moreover, YCF-2 reduced the level of nuclear-localized NF-κB (p65), which was increased by Aβ42 (Figure 9B). Consistently, when YCF-2 was added to BV-2 cells together with or prior to Aβ42, YCF-2 significantly decreased Aβ-mediated phosphorylated p65 (p-p65) levels at different time points (Figure 9C and D). These results suggested that YCF-2 blunted the transcriptional activity of NF-κB and down-regulated p65 phosphorylation and nuclear translocation, inhibiting the Aβ-induced production of proinflammatory mediators and microglial activation.

In summary, the novel chemical YCF-2 isolated from FBT, which consisted of kaempferol and the *p*-coumaroyl group, exhibited multiple properties by decreasing Aβ production, moderating Aβ oligomer structure, and mitigating Aβ-mediated cytotoxicity and neuroinflammation. This chemical offers a promising lead compound for the treatment of AD. Therefore, FBT, as a food supplement, might be effective in preventing and treating AD.

METHODS

Materials. Aβ42 was purchased from American Peptide Company (Sunnyvale, CA). Fuzhuan brick-tea (FBT, 3.6 kg) was from Yiyang Fu Cha Industry Development Co. Ltd., China. The following antibodies were used: A8717 (rabbit polyclonal raised against C-terminal of APP, C99, and C83; Sigma-Aldrich Corp. St. Louis, MO), 4G8 (monoclonal raised against Aβ17−24; Signet, MA), 6E10 (monoclonal raised against Aβ1−16; Cell Signaling, Beverly, MA), W20 (specific anti-Aβ oligomer scFv antibody, produced in our laboratory),[28] OC antibody (rabbit polyclonal raised against fibrillar oligomers; Invitrogen, Carlsbad, CA), A11 (rabbit polyclonal raised against prefibrillar oligomer; Invitrogen, Carlsbad, CA), anti-Iba-1 and anti-GFAP (GeneTex, Alton Pkwylrvine, CA), anti-p-p65 and p65 antibodies (Cell Signaling Technology, Beverly, MA), anti-β-actin (Sigma-Aldrich Corp. St. Louis, MO), HRP-9E10 (monoclonal raised against scFv; Santa Cruz Biotechnology, Inc., TX), and goat anti-mouse IgG HRP conjugate (Beijing Zhongshan Golden Bridge Biotechnology Co. Ltd., China). The Aβ40 and Aβ42 kits for Aβ measurement were purchased from IBL Co. Ltd. (Gunma, Japan). The BACE1 kit for activity detection was from BioVision (Milpitas, CA).

YCF-2 Isolation and Identification. FBT was extracted with 70% aqueous acetone, and the extracts were separated successively by petroleum ether, $CHCl_3$, and *n*-BuOH. The *n*-BuOH fraction was subjected to repeated Sephadex LH-20, ODS, MCI-gel, and polyamide CC to afford YCF-2 (8.6 mg). The isolated YCF-2 was identified by the IR spectra (Thermo), UV spectrum (Hitachi, Japan), ^{1}H and ^{13}C NMR, ^{1}H−^{1}H COSY, HSQC, HMBC, and ROESY spectra (Bruker AM-400), HRESI-MS (Thermo LTQ Orbitrap XL LC/MS), as well as by comparison of the spectral data with those of the reference. The configurations of the monosaccharides in YCF-2 were determined by acid hydrolysis, trimethylsilylimidazole derivation and GC-MS analysis on GCMS-QP2010S (Shimadzu, Japan), as previously described.[51]

HPLC Analysis of YCF-2. Approximately 2.5 g of FBT powder was saturated in 70% aqueous methanol (100 mL) for 12 h at room temperature, during which an ultrasonic bath was carried out twice for 15 min. The extract was filtered through a 0.22 μm membrane and named FBTE. FBTE was analyzed by HPLC with the eluent composed of mobile A (water containing 0.17% acetic acid) and mobile phase B (acetonitrile). The optimized gradient of mobile phase B was programmed as follows: 0−4 min, 6%; 4−16 min, from 6% to 14%; 16−18 min, from 14% to 15%; 18−32 min, from 15% to 18%; 32−34 min, 18%; 34−37 min, from 18% to 29%; 37−45 min, from 29% to 45%; 45−50 min, 45%; 50−60 min, from 45% to 6%; and maintained at 6% for 10 min. Elution was performed at a solvent flow rate of 1.0 mL/min.

Cell Culture. Chinese hamster ovary cells that were stably transfected to express mutant human APP (Val717Phe; cell line 7PA2) were a generous gift from Dr. Denis Selkoe, Harvard Medical School. The cells were cultured in Dulbecco's modified Eagle's medium (DMEM) supplemented with 10% (v/v) fetal bovine serum (FBS), antibiotics, and G418. HT22 hippocampal cells and BV-2 microglial cells were cultured in DMEM supplemented with 10% (v/v) FBS. Primary mixed glial cells were prepared from the cerebral cortex of Sprague−Dawley rat pups at postnatal day 1 and then maintained in DMEM/F12 containing 10% FBS for 6 days. The animal protocol used in our study was approved by the Institutional Review Board of Tsinghua University. All the cells were kept at 37 °C in a 5% CO_2-containing atmosphere.

Measurement of Aβ40 and Aβ42. To determine the effect of YCF-2 on Aβ production, 7PA2 cells were cultured with or without YCF-2, QC, or *p*-CA for 24 h. The amounts of Aβ40 and Aβ42 in the supernatant of the conditioned media were detected by sandwich ELISA using Aβ40 and Aβ42 immunoassay kits according to the manufacturer's recommendations.

BACE1 Activity Assay. To test the effect of YCF-2 on BACE1 activity, a commercial BACE1 kit was used according to the manufacturer's instructions. In brief, BACE1 enzyme incubated with different concentrations of YCF-2 (0, 10, 100, and 100 μM) for 20 min or lysate of 7PA2 cells treated with YCF-2, QC, and *p*-CA for 24 h was

DOI: 10.1021/acschemneuro.6b00091
ACS Chem. Neurosci. 2016, 7, 505−518

added into the reaction buffer containing β-secretase substrate (Mca-SEVNLDAEFRK(Dpn)RR-NH2). After 1 h of incubation at 37 °C, the fluorescence values were measured in a 96-well black plate using an MD-M5 microplate reader (Molecular Devices, Sunnyvale, CA) with excitation at 450 nm and emission at 482 nm.

Thioflavin T (ThT) Fluorescence and Congo Red (CR) Spectral Shift Assays. ThT dye and CR were used to determine the presence of amyloid aggregates. ThT fluorescence was measured as described previously.[28] The concentration of 20 μM of CR was added to the samples immediately before the assay. It was established that a ratio of 20 μM CR to 20 μM Aβ monomer and fibrils with or without YCF-2 resulted in the most detectable change in CR absorbance at 540 nm as a result of the presence of fibrils.

Transmission Electron Microscopy (TEM) Imaging. To prepare specimens for TEM imaging, a 10 μL aliquot of each sample was spotted onto a glow-discharged, carbon-coated Formvar grid and then incubated for 20 min. The droplet was displaced with an equal volume of 2.5% glutaraldehyde (v/v) and incubated for an additional 5 min. Finally, the grid was stained twice with 10 μL of uranyl acetate. The solution was wicked off, and the grid was air-dried. Samples were examined using a Hitachi H7650 TEM (Hitachi, Japan).

Circular Dichroism (CD) Spectroscopy. CD spectroscopy was used to detect the Aβ42 secondary structure according to a previously reported method with slight modification.[52] In brief, Aβ42 was dissolved in a freshly prepared buffer containing CH_3CN/Na_2CO_3 (300 μM)/NaOH (250 mM) (48.3:48.3:3.4, v/v/v) and diluted with PBS to 20 μM. CD measurements were performed on a J-715 spectropolarimeter (JASCO, Tokyo, Japan) with a 1 mm path length CD cuvette (Hellma, Forest Hills, NY, USA) containing 200 μL of samples. Spectra were recorded from 190 to 260 nm with a 2 nm bandwidth and 20 nm/min scan speed at 22 °C. Contributions of sample controls containing the above-mentioned buffer with or without addition of YCF-2 were subtracted from the CD spectra of Aβ42 coincubated with or without YCF-2, respectively. The percentages of secondary structures in the samples were estimated using the Protein Secondary Structure Estimation Program (Jasco Corp.)

ELISA, Western Blot, and Dot Blot. To measure Aβ42 oligomer levels in Aβ42 samples in the absence and presence of YCF-2, high-binding polystyrene microtiter plates were coated with 50 μL of preincubated samples at 4 °C overnight. Nonspecific binding was blocked by incubation with 3% (w/v) BSA at 37 °C for 2 h. The plates were then incubated with an oligomer-specific scFv antibody W20 or A11. Bound W20 and A11 were detected using a 1:1000 dilution of HRP-conjugated 9E10 and HRP-conjugated antirabbit IgG antibody, respectively.

Western blot was performed as described previously.[28] The samples were separated on SDS-PAGE gel, transferred onto a nitrocellulose membrane, blocked with 5% nonfat milk for 2 h at 37 °C, and incubated with the indicated antibodies diluted in TBS-T containing 3% nonfat milk for 1 h at RT. The membranes were washed again and incubated with the HRP-conjugated secondary antibody for 1 h at RT. The blots were developed with the ECL chemiluminescence kit (Pierce, Rockford, IL) as described by the manufacturer. The membranes were scanned, and the intensity of protein bands was quantified using ImageJ software (National Institutes of Health). To detect the levels of different Aβ forms after YCF-2 treatment, the incubated samples were applied to a nitrocellulose membrane (Millipore). The membrane was blocked with 5% milk in PBST and then incubated with W20, 6E10, and OC antibodies at RT for 1 h. The bound antibodies were correspondingly probed with HRP-conjugated goat anti-rabbit, 9E10, or goat anti-mouse/rabbit antibody. The immunoreactive blots were visualized with the ECL chemiluminescence kit. The intensity of each dot was quantified using ImageJ software (National Institutes of Health).

Molecular Dynamics Simulation. Molecular dynamics analysis was performed to determine which residues in YCF-2 contribute to the binding to Aβ42 or BACE1 enzyme. Initially, the unfolded and fully extended structures of YCF-2 were generated by PROTEIN program in Tinker software (backbone torsion φ, $\Psi = -135, 135$) using AMBER99 force field parameters to assign the atom types. The structure was then optimized by the Truncated Newton Conjugate Gradient method using the GB/SA continuum solvation model. Subsequently, 1 ns of molecular dynamics stimulation was carried out at a time step of 2.0 fs, and the system thermostat temperature was targeted to 298 K. Docking of YCF-2 to BACE1 or Aβ17−42 dimer was performed by customized script using PyRosetta. The result of docking was shown in PyMOL and further rendered with POV-RAY program.

MTT Assay. HT22 hippocampal cells were plated in 96-well polystyrene plates with approximately 2000 cells/100 μL of medium per well. Plates were incubated at 37 °C for 24 h to allow cells to attach. Aβ42 (20 μM) mixed with or without YCF-2, QC, and *p*-CA was diluted with fresh medium and added to individual wells. The final concentration of Aβ42 in each culture well was 2 μM. The same volume of medium was added to control cultures. The plates were then incubated for an additional 72 h at 37 °C. Cell viability was determined using an MTT toxicity assay with the addition of 10 μL of 5 mg/mL MTT to each well. After 4 h of incubation at 37 °C, the supernatants were replaced with a 150 μL aliquot of DMSO in the dark. An MD-M5 microplate reader was used to obtain the absorbance at 570 nm/630 nm. Averages from six replicate wells were used for each sample and control.

Lactate Dehydrogenase (LDH) Assay. HT22 hippocampal cells were plated in 96-well polystyrene plates. After seeding for 24 h, the culture medium was replaced with FBS-free medium, and Aβ42 mixed with or without YCF-2, QC, and *p*-CA was added into HT22 cells for 48 h of incubation. The supernatants were collected to measure the release of LDH using an assay kit (Roche Diagnostics, Indianapolis, IN) according to the manufacturer's instructions. In brief, 50 μL of centrifuged supernatants was added into 50 μL of reaction buffer and incubated for 30 min at room temperature. The leakage of LDH was assessed at OD 490 nm/655 nm. The control cells were incubated with 1% (v/v) Triton X-100 in FBS-free medium at 37 °C for 1 h to obtain maximum LDH release as a positive control with 100% cytotoxicity. The LDH release data represented at least three independent experiments.

TUNEL Staining. HT22 hippocampal cells were seeded on coverslips. After treatment with 4 μM Aβ42 or Aβ42 preincubated with YCF-2 for 24 h, the cells were washed with PBS. Apoptotic cells were evaluated by a TUNEL assay using an In Situ Cell Death Detection Kit, POD (Roche Diagnostics GmbH Mannheim, Germany) according to the manufacturer's instructions. The number of TUNEL-positive cells was counted in 10 randomized fields under a fluorescent microscope. Data analyses were performed using CXP 2.0 (Beckman Coulter, Inc., Indianapolis, IN).

Immunofluorescence. Primary mixed glial cells and BV-2 cells were seeded on coverslips. After treatment with 4 μM Aβ42 or Aβ42 preincubated with YCF-2, QC, or *p*-CA for the indicated time points, cells were washed with PBS and fixed with 4% paraformaldehyde for 20 min. After blocking with 10% FBS for 1 h, cells were incubated with appropriate primary antibodies at 37 °C for 1 h, incubated with second antibodies conjugated with fluorescent dyes for 1 h, and counter-stained with DAPI for 10 min. The number of activated microglial cells with large cell bodies was counted in 10 randomized fields by an Olympus BX60 microscope (Olympus Optical Co. Ltd., Tokyo, Japan) using IpWin5 analysis software.

Measurement of IL-6, TNF-α, and NO. BV-2 microglial cells were treated with 4 μM Aβ42 or Aβ42 preincubated with YCF-2 for 24 h. After incubation, the supernatants were collected, and the levels of IL-6, TNF-α, and NO released from activated BV-2 cells were determined by IL-6, TNF-α, and NO ELISA kits (R&D Systems, Minneapolis, MN) as described by the manufacturer's protocol. The absorbance was measured at 450 nm using an MD-M5 microplate reader.

Measurement of ROS. ROS production was fluorometrically monitored using 2′,7′-dichlorofluorescein diacetate (DCFH-DA) in BV-2 cells. Cells were treated with 4 μM Aβ42 in the absence or presence of 10 μM YCF-2, QC, or *p*-CA at 37 °C for 18 h. The cells were collected and washed with PBS three times. DCFH-DA was

DOI: 10.1021/acschemneuro.6b00091
ACS Chem. Neurosci. 2016, 7, 505−518

diluted in fresh DMEM (without phenol red) to a final concentration of 5 μM and then incubated with the cells for 30 min at 37 °C. The chemicals were then removed, and the cells were washed three times with PBS. Relative ROS units were determined using an MD-M5 microplate reader (excitation at 485 nm, emission at 530 nm). ROS production was expressed as a percentage of the control sample. The fluorescence of DCFH-DA in BV-2 cells was detected with a confocal laser scanning microscope (OLYMPUS BX61).

Luciferase Assay. BV-2 cells were transiently transfected with the indicated plasmids using Vigofect according to the manufacturer's instructions. In brief, 0.1 μg of reporter plasmid pGL3/NF-κB-luc together with 5 ng of the internal control plasmid pRL-TK were cotransfected into BV-2 cells. The cells were then treated with 4 μM Aβ42 or Aβ42 preincubated with 10 μM YCF-2, QC, or *p*-CA at 37 °C for 18 h. The cells were collected and washed with PBS three times. Luciferase activity was assayed using a Dual-Luciferase reporter assay system. Firefly luciferase activity was normalized against *Renilla* luciferase activity.

Statistics. The data presented in this study were obtained from at least three independent experiments for each experimental condition. Data were expressed as the mean ± SD, and their statistical significance was analyzed by one-way ANOVA. Multiple comparisons were performed by Duncan's test.

■ ASSOCIATED CONTENT

Supporting Information

The Supporting Information is available free of charge on the ACS Publications website at DOI: 10.1021/acschemneuro.6b00091.

Structure identification of camellikaempferoside B (YCF-2) (PDF)

■ AUTHOR INFORMATION

Corresponding Authors

*(R.-t.L.) E-mail: rtliu@home.ipe.ac.cn. National Key Laboratory of Biochemical Engineering, Institute of Process Engineering, Chinese Academy of Sciences, Haidian District, Beijing 100190, China. Tel.: +86 10 82545017. Fax: +86 10 82545025.

*(T.-j.L.) E-mail: lingtj@ahau.edu.cn. State Key Laboratory of Tea Plant Biology and Utilization, Anhui Agricultural University, Hefei 230036, China. Tel.: +86 551 5786401. Fax: +86 551 5786765.

*(W.-y.W.) E-mail: weiyunw@ahau.edu.cn. School of Life Science, Anhui Agricultural University, Hefei 230036, China. Tel.: +86 551 5786639. Fax: +86 551 5786293.

Author Contributions

‖S.Y., W.L., and and S.L. contributed equally to this work.

Funding

This work was supported by grants from the National Natural Science Foundation of China (Grant Nos. 81371208, 81171014, and 31471720) and the National Science and Technology Major Projects of New Drugs (Grant Nos. 2012ZX09103301-001 and 2014ZX09102045-006).

Notes

The authors declare no competing financial interest.

■ ABBREVIATIONS

AD, Alzheimer's disease; Aβ, β-amyloid; FBT, Fuzhuan brick tea; CD, circular dichroism; TEM, transmission electron microscopy; ThT, thioflavin T; HFIP, 1,1,1,3,3,3-hexafluoro-2-propanal; SDS-PAGE, sodium dodecyl sulfate-polyacrylamide gel electrophoresis; BACE1, amyloid precursor protein cleaving enzyme 1; APP, β-amyloid precursor protein; MTT, 3-(4,5-dimethylthiazol-2-yl)-2,5-diphenyltetrazolium bromide; ROS, reactive oxygen species; IL-1β, interleukin-1β; IL-6, interleukin-6; NO, nitric oxide; Iba-1, ionized calcium binding adaptor molecule-1; GFAP, glial fibrillary acidic protein

■ REFERENCES

(1) Jakob-Roetne, R., and Jacobsen, H. (2009) Alzheimer's disease: from pathology to therapeutic approaches. *Angew. Chem., Int. Ed. 48*, 3030−3059.

(2) De Strooper, B., Vassar, R., and Golde, T. (2010) The secretases: enzymes with therapeutic potential in Alzheimer disease. *Nat. Rev. Neurol. 6*, 99−107.

(3) Hardy, J., and Selkoe, D. J. (2002) The amyloid hypothesis of Alzheimer's disease: progress and problems on the road to therapeutics. *Science 297*, 353−356.

(4) Malaplate-Armand, C., Florent-Bechard, S., Youssef, I., Koziel, V., Sponne, I., Kriem, B., Leininger-Muller, B., Olivier, J. L., Oster, T., and Pillot, T. (2006) Soluble oligomers of amyloid-beta peptide induce neuronal apoptosis by activating a cPLA2-dependent sphingomyelinase-ceramide pathway. *Neurobiol. Dis. 23*, 178−189.

(5) Yao, M., Nguyen, T. V., and Pike, C. J. (2005) Beta-amyloid-induced neuronal apoptosis involves c-Jun N-terminal kinase-dependent downregulation of Bcl-w. *J. Neurosci. 25*, 1149−1158.

(6) Floden, A. M., Li, S., and Combs, C. K. (2005) Beta-amyloid-stimulated microglia induce neuron death via synergistic stimulation of tumor necrosis factor alpha and NMDA receptors. *J. Neurosci. 25*, 2566−2575.

(7) Luo, X. G., Ding, J. Q., and Chen, S. D. (2010) Microglia in the aging brain: relevance to neurodegeneration. *Mol. Neurodegener. 5*, 12.

(8) Tamagno, E., Guglielmotto, M., Aragno, M., Borghi, R., Autelli, R., Giliberto, L., Muraca, G., Danni, O., Zhu, X., Smith, M. A., Perry, G., Jo, D. G., Mattson, M. P., and Tabaton, M. (2008) Oxidative stress activates a positive feedback between the gamma- and beta-secretase cleavages of the beta-amyloid precursor protein. *J. Neurochem. 104*, 683−695.

(9) Lesne, S., Koh, M. T., Kotilinek, L., Kayed, R., Glabe, C. G., Yang, A., Gallagher, M., and Ashe, K. H. (2006) A specific amyloid-beta protein assembly in the brain impairs memory. *Nature 440*, 352−357.

(10) Shankar, G. M., Li, S., Mehta, T. H., Garcia-Munoz, A., Shepardson, N. E., Smith, I., Brett, F. M., Farrell, M. A., Rowan, M. J., Lemere, C. A., Regan, C. M., Walsh, D. M., Sabatini, B. L., and Selkoe, D. J. (2008) Amyloid-beta protein dimers isolated directly from Alzheimer's brains impair synaptic plasticity and memory. *Nat. Med. 14*, 837−842.

(11) Block, M. L., Zecca, L., and Hong, J. S. (2007) Microglia-mediated neurotoxicity: uncovering the molecular mechanisms. *Nat. Rev. Neurosci. 8*, 57−69.

(12) Frank-Cannon, T. C., Alto, L. T., McAlpine, F. E., and Tansey, M. G. (2009) Does neuroinflammation fan the flame in neurodegenerative diseases? *Mol. Neurodegener. 4*, 47.

(13) Glass, C. K., Saijo, K., Winner, B., Marchetto, M. C., and Gage, F. H. (2010) Mechanisms underlying inflammation in neurodegeneration. *Cell 140*, 918−934.

(14) Longpre, F., Garneau, P., Christen, Y., and Ramassamy, C. (2006) Protection by EGb 761 against beta-amyloid-induced neurotoxicity: involvement of NF-kappaB, SIRT1, and MAPKs pathways and inhibition of amyloid fibril formation. *Free Radical Biol. Med. 41*, 1781−1794.

(15) Yang, S., Wang, Y., Mei, K., Zhang, S., Sun, X., Ren, F., Liu, S., Yang, Z., Wang, X., Qin, Z., and Chang, Z. (2015) Tumor necrosis factor receptor 2 (TNFR2).interleukin-17 receptor D (IL-17RD) heteromerization reveals a novel mechanism for NF-kappaB activation. *J. Biol. Chem. 290*, 861−871.

(16) Zhou, W. W., Lu, S., Su, Y. J., Xue, D., Yu, X. L., Wang, S. W., Zhang, H., Xu, P. X., Xie, X. X., and Liu, R. T. (2014) Decreasing oxidative stress and neuroinflammation with a multifunctional peptide rescues memory deficits in mice with Alzheimer disease. *Free Radical Biol. Med. 74*, 50−63.

DOI: 10.1021/acschemneuro.6b00091
ACS Chem. Neurosci. 2016, 7, 505−518

(17) Neumann, U., Rueeger, H., Machauer, R., Veenstra, S. J., Lueoend, R. M., Tintelnot-Blomley, M., Laue, G., Beltz, K., Vogg, B., Schmid, P., Frieauff, W., Shimshek, D. R., Staufenbiel, M., and Jacobson, L. H. (2015) A novel BACE inhibitor NB-360 shows a superior pharmacological profile and robust reduction of amyloid-beta and neuroinflammation in APP transgenic mice. *Mol. Neurodegener. 10*, 44.
(18) Olea, R. S. G., Roque, N. F., and Bolzani, V. d. S. (1997) Acylated flavonol glycosides and terpenoids from the leaves of Alibertia sessilis. *J. Braz. Chem. Soc. 8*, 257−259.
(19) Vassar, R. (2014) BACE1 inhibitor drugs in clinical trials for Alzheimer's disease. *Alzheimer's Res. Ther. 6*, 89.
(20) Reardon, S. (2015) Antibody drugs for Alzheimer's show glimmers of promise. *Nature 523*, 509−510.
(21) Xu, P. X., Wang, S. W., Yu, X. L., Su, Y. J., Wang, T., Zhou, W. W., Zhang, H., Wang, Y. J., and Liu, R. T. (2014) Rutin improves spatial memory in Alzheimer's disease transgenic mice by reducing Abeta oligomer level and attenuating oxidative stress and neuroinflammation. *Behav. Brain Res. 264*, 173−180.
(22) Wang, S. W., Yang, S. G., Liu, W., Zhang, Y. X., Xu, P. X., Wang, T., Ling, T. J., and Liu, R. T. (2016) Alpha-tocopherol quinine ameliorates spatial memory deficits by reducing beta-amyloid oligomers, neuroinflammation and oxidative stress in transgenic mice with Alzheimer's disease. *Behav. Brain Res. 296*, 109−117.
(23) Xue, D., Zhao, M., Wang, Y. J., Wang, L., Yang, Y., Wang, S. W., Zhang, R., Zhao, Y., and Liu, R. T. (2012) A multifunctional peptide rescues memory deficits in Alzheimer's disease transgenic mice by inhibiting Abeta42-induced cytotoxicity and increasing microglial phagocytosis. *Neurobiol. Dis. 46*, 701−709.
(24) Yang, S. G., Wang, W. Y., Ling, T. J., Feng, Y., Du, X. T., Zhang, X., Sun, X. X., Zhao, M., Xue, D., and Yang, Y. (2010) alpha-Tocopherol quinone inhibits beta-amyloid aggregation and cytotoxicity, disaggregates preformed fibrils and decreases the production of reactive oxygen species, NO and inflammatory cytokines. *Neurochem. Int. 57*, 914−922.
(25) Yang, S. G., Zhang, X., Sun, X. S., Ling, T. J., Feng, Y., Du, X. Y., Zhao, M., Yang, Y., Xue, D., Wang, L., and Liu, R. T. (2010) Diverse ecdysterones show different effects on amyloid-beta42 aggregation but all uniformly inhibit amyloid-beta42-induced cytotoxicity. *J. Alzheimer's Dis. 22*, 107−117.
(26) Sciarretta, K. L., Gordon, D. J., and Meredith, S. C. (2006) Peptide-based inhibitors of amyloid assembly. *Methods Enzymol. 413*, 273−312.
(27) Yang, S. G., Wang, S. W., Zhao, M., Zhang, R., Zhou, W. W., Li, Y. N., Su, Y. J., Zhang, H., Yu, X. L., and Liu, R. T. (2012) A peptide binding to the beta-site of APP improves spatial memory and attenuates Abeta burden in Alzheimer's disease transgenic mice. *PLoS One 7*, e48540.
(28) Wang, X. P., Zhang, J. H., Wang, Y. J., Feng, Y., Zhang, X., Sun, X. X., Li, J. L., Du, X. T., Lambert, M. P., Yang, S. G., Zhao, M., Klein, W. L., and Liu, R. T. (2009) Conformation-dependent single-chain variable fragment antibodies specifically recognize beta-amyloid oligomers. *FEBS Lett. 583*, 579−584.
(29) Morgado, I., Wieligmann, K., Bereza, M., Ronicke, R., Meinhardt, K., Annamalai, K., Baumann, M., Wacker, J., Hortschansky, P., Malesevic, M., Parthier, C., Mawrin, C., Schiene-Fischer, C., Reymann, K. G., Stubbs, M. T., Balbach, J., Gorlach, M., Horn, U., and Fandrich, M. (2012) Molecular basis of beta-amyloid oligomer recognition with a conformational antibody fragment. *Proc. Natl. Acad. Sci. U. S. A. 109*, 12503−12508.
(30) Ehrnhoefer, D. E., Bieschke, J., Boeddrich, A., Herbst, M., Masino, L., Lurz, R., Engemann, S., Pastore, A., and Wanker, E. E. (2008) EGCG redirects amyloidogenic polypeptides into unstructured, off-pathway oligomers. *Nat. Struct. Mol. Biol. 15*, 558−566.
(31) Rezai-Zadeh, K., Shytle, D., Sun, N., Mori, T., Hou, H., Jeanniton, D., Ehrhart, J., Townsend, K., Zeng, J., Morgan, D., Hardy, J., Town, T., and Tan, J. (2005) Green tea epigallocatechin-3-gallate (EGCG) modulates amyloid precursor protein cleavage and reduces cerebral amyloidosis in Alzheimer transgenic mice. *J. Neurosci. 25*, 8807−8814.
(32) Marambaud, P., Zhao, H., and Davies, P. (2005) Resveratrol promotes clearance of Alzheimer's disease amyloid-beta peptides. *J. Biol. Chem. 280*, 37377−37382.
(33) Ge, J. F., Qiao, J. P., Qi, C. C., Wang, C. W., and Zhou, J. N. (2012) The binding of resveratrol to monomer and fibril amyloid beta. *Neurochem. Int. 61*, 1192−1201.
(34) Yanagisawa, D., Taguchi, H., Yamamoto, A., Shirai, N., Hirao, K., and Tooyama, I. (2011) Curcuminoid binds to amyloid-beta1−42 oligomer and fibril. *J. Alzheimer's Dis. 24* (Suppl 2), 33−42.
(35) Kim, H., Park, B. S., Lee, K. G., Choi, C. Y., Jang, S. S., Kim, Y. H., and Lee, S. E. (2005) Effects of naturally occurring compounds on fibril formation and oxidative stress of beta-amyloid. *J. Agric. Food Chem. 53*, 8537−8541.
(36) Shimmyo, Y., Kihara, T., Akaike, A., Niidome, T., and Sugimoto, H. (2008) Flavonols and flavones as BACE-1 inhibitors: structure-activity relationship in cell-free, cell-based and in silico studies reveal novel pharmacophore features. *Biochim. Biophys. Acta, Gen. Subj. 1780*, 819−825.
(37) Ansari, M. A., Abdul, H. M., Joshi, G., Opii, W. O., and Butterfield, D. A. (2009) Protective effect of quercetin in primary neurons against Abeta(1−42): relevance to Alzheimer's disease. *J. Nutr. Biochem. 20*, 269−275.
(38) Lu, J., Wu, D. M., Zheng, Y. L., Hu, B., Zhang, Z. F., Shan, Q., Zheng, Z. H., Liu, C. M., and Wang, Y. J. (2010) Quercetin activates AMP-activated protein kinase by reducing PP2C expression protecting old mouse brain against high cholesterol-induced neurotoxicity. *Journal of pathology 222*, 199−212.
(39) Youn, K., and Jun, M. (2012) Inhibitory effects of key compounds isolated from Corni fructus on BACE1 Activity. *Phytother. Res. 26*, 1714−1718.
(40) Cohen, S. I., Linse, S., Luheshi, L. M., Hellstrand, E., White, D. A., Rajah, L., Otzen, D. E., Vendruscolo, M., Dobson, C. M., and Knowles, T. P. (2013) Proliferation of amyloid-beta42 aggregates occurs through a secondary nucleation mechanism. *Proc. Natl. Acad. Sci. U. S. A. 110*, 9758−9763.
(41) Lee, J., Culyba, E. K., Powers, E. T., and Kelly, J. W. (2011) Amyloid-beta forms fibrils by nucleated conformational conversion of oligomers. *Nat. Chem. Biol. 7*, 602−609.
(42) Kayed, R., Head, E., Sarsoza, F., Saing, T., Cotman, C. W., Necula, M., Margol, L., Wu, J., Breydo, L., Thompson, J. L., Rasool, S., Gurlo, T., Butler, P., and Glabe, C. G. (2007) Fibril specific, conformation dependent antibodies recognize a generic epitope common to amyloid fibrils and fibrillar oligomers that is absent in prefibrillar oligomers. *Mol. Neurodegener. 2*, 18.
(43) Kayed, R., Head, E., Thompson, J. L., McIntire, T. M., Milton, S. C., Cotman, C. W., and Glabe, C. G. (2003) Common structure of soluble amyloid oligomers implies common mechanism of pathogenesis. *Science 300*, 486−489.
(44) Ryan, T. M., Roberts, B. R., McColl, G., Hare, D. J., Doble, P. A., Li, Q. X., Lind, M., Roberts, A. M., Mertens, H. D., Kirby, N., Pham, C. L., Hinds, M. G., Adlard, P. A., Barnham, K. J., Curtain, C. C., and Masters, C. L. (2015) Stabilization of nontoxic Abeta-oligomers: insights into the mechanism of action of hydroxyquinolines in Alzheimer's disease. *J. Neurosci. 35*, 2871−2884.
(45) Ahmed, M., Davis, J., Aucoin, D., Sato, T., Ahuja, S., Aimoto, S., Elliott, J. I., Van Nostrand, W. E., and Smith, S. O. (2010) Structural conversion of neurotoxic amyloid-beta(1−42) oligomers to fibrils. *Nat. Struct. Mol. Biol. 17*, 561−567.
(46) Du, W. J., Guo, J. J., Gao, M. T., Hu, S. Q., Dong, X. Y., Han, Y. F., Liu, F. F., Jiang, S., and Sun, Y. (2015) Brazilin inhibits amyloid beta-protein fibrillogenesis, remodels amyloid fibrils and reduces amyloid cytotoxicity. *Sci. Rep. 5*, 7992.
(47) Yoon, J. H., Youn, K., Ho, C. T., Karwe, M. V., Jeong, W. S., and Jun, M. (2014) p-Coumaric acid and ursolic acid from Corni fructus attenuated beta-amyloid(25−35)-induced toxicity through regulation of the NF-kappaB signaling pathway in PC12 cells. *J. Agric. Food Chem. 62*, 4911−4916.

DOI: 10.1021/acschemneuro.6b00091
ACS Chem. Neurosci. 2016, 7, 505−518

(48) Ma, J. Q., Li, Z., Xie, W. R., Liu, C. M., and Liu, S. S. (2015) Quercetin protects mouse liver against CCl-induced inflammation by the TLR2/4 and MAPK/NF-kappaB pathway. *Int. Immunopharmacol. 28*, 531−539.
(49) Huang, R., Zhong, T., and Wu, H. (2015) Quercetin protects against lipopolysaccharide-induced acute lung injury in rats through suppression of inflammation and oxidative stress. *Arch. Med. Sci. 11*, 427−432.
(50) Pragasam, S. J., and Rasool, M. (2013) Dietary component p-coumaric acid suppresses monosodium urate crystal-induced inflammation in rats. *Inflammation Res. 62*, 489−498.
(51) Zong, J., Wang, R., Bao, G., Ling, T., Zhang, L., Zhang, X., and Hou, R. (2015) Novel triterpenoid saponins from residual seed cake of Camellia oleifera Abel. show anti-proliferative activity against tumor cells. *Fitoterapia 104*, 7−13.
(52) Bartolini, M., Bertucci, C., Bolognesi, M. L., Cavalli, A., Melchiorre, C., and Andrisano, V. (2007) Insight into the kinetic of amyloid beta (1−42) peptide self-aggregation: elucidation of inhibitors' mechanism of action. *ChemBioChem 8*, 2152−2161.

■ NOTE ADDED AFTER ASAP PUBLICATION

This paper was published ASAP on April 8, 2016 with an error in Figure 1. The corrected version was reposted to the web on April 11, 2016.

DOI: 10.1021/acschemneuro.6b00091
ACS Chem. Neurosci. 2016, 7, 505−518